Ab Initio and RRKM Calculations for Multichannel Rate Constants of the $C_2H_3 + O_2$ Reaction

A. M. Mebel, E. W. G. Diau, M. C. Lin,* and K. Morokuma*

Contribution from the Cherry L. Emerson Center for Scientific Computation and Department of Chemistry, Emory University, Atlanta, Georgia 30322

Received May 3, 1996. Revised Manuscript Received July 5, 1996[⊗]

Abstract: A potential energy surface for the reaction of vinyl radical with molecular oxygen has been studied using the ab initio G2M(RCC,MP2) method. The most favorable reaction pathway leading to the major CHO + CH_2O products is the following: $C_2H_3 + O_2$ → vinylperoxy radical **1** or **1′** → TS **8** → dioxiranylmethyl radical **3** → TS **9′** oxiranyloxy radical **10** → TS **11** → formyloxymethyl radical **12′** → TS **13′** → CHO + CH_2O, where the rate-determining step is oxygen migration to the CC bridging position via TS **9′**, lying below the reactants by 14.3 kcal/mol. The C_2H_3O + O products can be formed by elimination of the oxygen atom from C_2H_3OO via TS **23**, which is by 7.8 kcal/mol lower in energy than the reactants, but by 6.5 kcal/mol higher than TS **9′**. The hydrogen migration in **1′** gives rise to another significant product channel: $C_2H_3 + O_2$ → **1′** → TS **25′** → $C_2H_2 + O_2H$, with TS **25′** lying below $C_2H_3 + O_2$ by 3.5 kcal/mol. Multichannel RRKM calculations have been carried out for the total and individual rate constants for various channels using the G2M(RCC,MP2) energetics and molecular parameters of the intermediates and transition states. The computed low pressure reaction rate constant is in quantitative agreement with experiment. At atmospheric pressure, the title reaction is dominated by the stabilization of vinylperoxy radical C_2H_3OO at room temperature. In the 500−900 K temperature range, the CHO + CH_2O channel has the highest rate constant, and at $T \geq 900$ K, C_2H_3O + O are the major products. At very high temperatures, the channel producing $C_2H_2 + O_2H$ becomes competitive.

I. Introduction

Vinyl radicals play an important role in hydrocarbon-fuel combustion reactions. Its successive reaction products with C_2H_2, for example, have been shown to be a potential source of benzene,[1] the building block of PAH's (polycyclic aromatic hydrocarbons), precursors to soot.[2−4]

The reaction of C_2H_3 with O_2 retards soot formation by effectively competing with C_2H_4 and other unsaturated hydrocarbons. The reaction is also a key step in the high-temperature oxidation of C_2H_4 and in C_2H_2 and C_2H_4 flames.[5−7] Because of the high reactivity[8−12] and exothermicity of the $C_2H_3 + O_2$ reaction, many product channels may be accessible, particularly under high-temperature combustion conditions, viz.:

$$\begin{aligned} C_2H_3 + O_2 &\rightarrow C_2H_3OO + 46.4 \text{ kcal/mol} \\ &\rightarrow C_2H_3O + O + 9.0 \text{ kcal/mol} \\ &\rightarrow CHO + CH_2O + 87.5 \text{ kcal/mol} \\ &\rightarrow C_2H_2 + HO_2 + 13.4 \text{ kcal/mol} \\ &\rightarrow CH_2CO + OH + 0.6 \text{ kcal/mol} \\ &\rightarrow C_2H_2O_2 + H + 77.1 \text{ kcal/mol} \\ &\rightarrow CH_3 + CO_2 + 131.1 \text{ kcal/mol} \end{aligned}$$

Most of these exothermic product channels may contribute significantly and variably over a wide range of temperature and pressure. Our goal is to quantify their relative contributions using a combined high-level ab initio molecular orbital and statistical rate constant (RRKM) calculation for the respective transition states and associated products in order to provide a reliable estimate of these rate constants for practical combustion applications.

Gutman, Slagle, and co-workers[8,9] showed experimentally that the $C_2H_3 + O_2$ reaction produces predominantly the CHO + CH_2O products below 1000 K. How the yields of these and other products would change with temperature and pressure under combustion conditions is not easy to speculate without a sound theoretical basis. To answer this important question, Westmoreland[13] as well as Bozzelli and Dean[14] have employed a version of RRK theory to calculate the branching ratios of several of these products using assumed Arrhenius parameters. These exercises are useful for a qualitative guidance but may be dangerous because the calculated data are very sensitive to the assumed parameters. Also, the process is complex as will be illustrated later for a specific case of the title reaction.

Recently, Carpenter[15] has carried out semiempirical and ab initio molecular orbital (MO) calculations of the potential energy surface of the $C_2H_3 + O_2$ reaction. He suggested the existence of a new reaction mechanism involving cyclization of the first-

[⊗] Abstract published in *Advance ACS Abstracts,* September 15, 1996.

(1) Callear, A. B.; Smith, G. B. *J. Phys. Chem.* **1986**, *90*, 3229.
(2) Glassman, I. *Combustion*, 2nd ed.; Academic Press: New York, 1986.
(3) Wang, H.; Frenklach, M. *J. Phys. Chem.* **1994**, *98*, 11465.
(4) Bittner, J. D.; Howard, J. B.; Palmer, H. B. *NATO Conference Series, 6: Materials Science*; Plenum Press: New York, 1983; Vol. 7, p 95.
(5) Böhm, H.; Feldermann, C.; Heidermann, T.; Jander, H.; Lüters, B.; Wagner, H. Gg. *Twenty-Fourth Symposium (International) on Combustion*; The Combustion Institute: Pittsburgh, PA, 1992; p 991.
(6) Volponi, J. V.; Branch, M. C. *Twenty-Fourth Symposium (International) on Combustion*; The Combustion Institute: Pittsburgh, PA, 1992; p 823.
(7) Chen, N.-H.; Rogg, B.; Bray, K. N. C. *Twenty-Fourth Symposium (International) on Combustion*; The Combustion Institute: Pittsburgh, PA, 1992; p 1513.
(8) Park, J.-Y.; Heaven, M. C.; Gutman, D. *Chem. Phys. Lett.* **1984**, *104*, 469.
(9) Slagle, I. R.; Park, J.-Y.; Heaven, M. C.; Gutman, D. *J. Am. Chem. Soc.* **1984**, *106*, 4356.
(10) Krueger, H.; Weitz, E. *J. Chem. Phys.* **1988**, *88*, 1608.
(11) Fahr, A.; Laufer, A. H. *J. Phys. Chem.* **1988**, *92*, 7229.
(12) Knyazev, V. D.; Slagle, I. R. *J. Phys. Chem.* **1995**, *99*, 2247.
(13) Westmoreland, P. R. *Combust. Sci. Technol.* **1992**, *82*, 151.
(14) Bozzelli, J. W.; Dean, A. M. *J. Phys. Chem.* **1993**, *97*, 4427.
(15) (a) Carpenter, B. K. *J. Am. Chem. Soc.* **1993**, *115*, 9806. (b) Carpenter, B. K. *J. Phys. Chem.* **1995**, *99*, 9801.

S0002-7863(96)01476-X CCC: $12.00

formed vinylperoxy radical to a three-member-ring dioxiranyl radical rather than the four-member-ring dioxetanyl radical which was assumed in earlier mechanisms.[8,9,16] However, Carpenter's consideration of the reaction mechanisms is far from complete. The theoretical method he used, PMP4(SDTQ)/6-311G(d)//UMP2/6-311G(d), may provide a qualitative description of the potential energy surface but may not give quantitatively accurate data, especially for systems with spin contamination of such magnitude as $C_2H_3 + O_2$.

In this paper, we present a detailed ab initio MO study of nearly all possible channels of the title reaction including the consideration of various intermediates of the $C_2H_3O_2$ radical. As will be discussed below, we use our newly established G2M(RCC,MP2) method,[17] which is designed to give energies of radical intermediates and transition states to experimental accuracy. The ab initio MO data are employed for the RRKM calculations of the multichannel rate constants which are compared with experimental results.

II. Calculation Methods

The geometries of the reactants, products, various intermediates, and transition states for the $C_2H_3 + O_2$ reaction have been optimized using the hybrid density functional B3LYP method, i.e., Becke's three-parameter nonlocal-exchange functional[18] with the nonlocal correlation functional of Lee, Yang, and Parr,[19] with the 6-311G(d,p) basis set.[20] Vibrational frequencies, calculated at the B3LYP/6-311G(d,p) level, have been used for characterization of stationary points, zero-point energy (ZPE) correction, and RRKM computations. All the stationary points have been positively identified for minimum (number of imaginary frequencies (NIMAG) = 0) or transition state (NIMAG = 1). Connections of the transition states between designated intermediates have been confirmed by intrinsic reaction coordinate (IRC) calculations[21] at the B3LYP level. All the energies quoted and discussed in the present paper include the ZPE correction.

In order to obtain more reliable energies of the most important intermediates and transition states, we used the MP4(SDTQ)/6-311G(d,p), MP4(SDTQ)/6-311+G(d,p),[20] and G2M(RCC,MP2)[17] methods. The G2M(RCC,MP2) method is a modification of the Gaussian-2 (G2) approach[22] by Pople and co-workers, it uses B3LYP/6-311(G(d,p) optimized geometries and ZPE corrections and substitutes the QCISD(T)/6-311G(d,p) calculation of the original G2 scheme by the restricted open shell coupled cluster[23] RCCSD(T)/6-311G(d,p) calculation. The total energy in G2M(RCC,MP2) is calculated as follows:[17]

$$E[\text{G2M(RCC,MP2)}] = E[\text{RCCSD(T)/6-311G(d,p)}] + \Delta E(+3\text{df2p}) + \Delta E(\text{HLC}) + \text{ZPE[B3LYP/6-311G(d,p)]}$$

where

$$\Delta E(+3\text{df2p}) = E[\text{MP2/6-311+G(3df,2p)}] - E[\text{MP2/6-311G(d,p)}]$$

and the empirical "higher level correction"

$$\Delta E(\text{HLC}) = -5.25n_\beta - 0.19n_\alpha$$

where n_α and n_β are the number of α and β valence electrons, respectively. It has been shown[17] that the G2M(RCC,MP2) method gives the average absolute deviation of 1.15 kcal/mol of calculated atomization energies from experiment for 32 first-row G2 test compounds. The preference of the G2M(RCC) methods over original G2 is expected to be particularly significant for the open-shell systems with large spin contamination. For some structures we carried out CASSCF calculations.[24] The GAUSSIAN 92/DFT,[25] MOLPRO 94,[26] and GAMESS[27] programs were employed for the potential energy surface computations.

Rice−Ramsperger−Kassel−Marcus (RRKM) calculations have been carried out for the total and individual rate constants using the equations described earlier[28−30] and a modified multichannel computer program previously written for the $CH_3 + O_2$ reaction.[30]

III. Results and Discussion

The structures of all the reactants, products, intermediates, and transition states calculated in the present paper are shown in Figure 1. The profile of the potential energy surface for important channels of the $C_2H_3 + O_2$ reaction at the B3LYP/6-311G(d,p) + ZPE is shown in Figure 2. The energies at the more quantitative G2M(RCC,MP2) are numerically shown for some structures in Figure 2.

The reaction of C_2H_3 with O_2 starts by the formation of vinylperoxy radical, C_2H_3OO, when the oxygen molecule attaches to the radical site of the vinyl radical. As will be discussed later, the direct abstraction paths, either $C_2H_3 + O_2 \rightarrow C_2H_3O + O$ or $C_2H_3 + O_2 \rightarrow C_2H_2 + O_2H$, do not exist. In C_2H_3OO, the radical center is shifted to the π-orbital of the terminal oxygen, and the CC bond retains its double character. As could be anticipated for the reaction of the radicals, no transition states were found on the $C_2H_3 + O_2 \rightarrow C_2H_3OO$ potential energy surface. The vinylperoxy radical can be created from the reactants in two stable conformations: **1**, with the OO bond in the *trans*-position toward CC, and **1′**, with OO in the *cis*-position. Both **1** and **1′** have C_s symmetry and $^2A''$ electronic state. **1** is 1.2 kcal/mol more favorable than **1′**. The exothermicity of C_2H_3OO formation at the first reaction step is calculated to be 45.2−46.4 kcal/mol at the G2M(RCC,MP2) level. The B3LYP optimized geometry of the *trans*-C_2H_3OO, **1**, is similar to that obtained by Carpenter at the UMP2 level. The PMP4/6-311G(d)+ZPE energy difference of 33.1 kcal/mol between $C_2H_3 + O_2$ and **1** reported by Carpenter is significantly underestimated as compared to higher levels of theory.

A. Four-Member-Ring Reaction Mechanism. Baldwin and Walker proposed[16] the mechanism of CHO + CH_2O formation involving a four-member-ring intermediate **2**. This mechanism served a long time as the basis for description of

(16) Baldwin, R. R.; Walker, R. W. *Eighteenth Symposium (International) on Combustion*; The Combustion Institute: Pittsburgh, PA, 1981; p 819.
(17) Mebel, A. M.; Morokuma, K.; Lin, M. C. *J. Chem. Phys.* **1995**, *103*, 7414.
(18) (a) Becke, A. D. *J. Chem. Phys.* **1993**, *98*, 5648. (b) Becke, A. D. *J. Chem. Phys.* **1992**, *96*, 2155. (c) Becke, A. D. *J. Chem. Phys.* **1992**, *97*, 9173.
(19) Lee, C.; Yang, W.; Parr, R. G. *Phys. Rev.* **1988**, *B37*, 785.
(20) Hehre, W.; Radom, L.; Schleyer, P. v. R.; Pople, J. A. *Ab Initio Molecular Orbital Theory*; Wiley: New York, 1986.
(21) Gonzalez, C.; Schlegel, H. B. *J. Phys. Chem.* **1989**, *90*, 2154.
(22) (a) Pople, J. A.; Head-Gordon, M.; Fox, D. J.; Raghavachari, K.; Curtiss, L. A. *J. Chem. Phys.* **1989**, *90*, 5622. (b) Curtiss, L. A.; Jones, C.; Trucks, G. W.; Raghavachari, K.; Pople, J. A. *J. Chem. Phys.* **1990**, *93*, 2537. (c) Curtiss, L. A.; Raghavachari, K.; Trucks, G. W.; Pople, J. A. *J. Chem. Phys.* **1991**, *94*, 7221. (d) Curtiss, L. A.; Raghavachari, K.; Trucks, G. W.; Pople, J. A. *J. Chem. Phys.* **1993**, *98*, 1293.
(23) (a) Purvis, G. D.; Bartlett, R. J. *J. Chem. Phys.* **1982**, *76*, 1910. (b) Hampel, C.; Peterson, K. A.; Werner, H.-J. *Chem. Phys. Lett.* **1992**, *190*, 1. (c) Knowles, P. J.; Hampel, C.; Werner, H.-J. *J. Chem. Phys.* **1994**, *99*, 5219. (d) Deegan, M. J. O.; Knowles, P. J. *Chem. Phys. Lett.* **1994**, *99*, 321.
(24) Eade, R. H. E.; Robb, M. A. *Chem. Phys. Lett.* **1981**, *83*, 362.
(25) Frisch, M. J.; Trucks, G. W.; Head-Gordon, M.; Gill, P. M. W.; Wong, M. W.; Foresman, J. B.; Johnson, B. G.; Schlegel, H. B.; Robb, M. A.; Reglogle, E. S.; Gomperts, R.; Andres, J. L.; Raghavachari, K.; Binkley, J. S.; Gonzales, C.; Martin, R. L.; Fox, D. J.; DeFrees, D. J.; Baker, J.; Stewart, J. J. P.; Pople, J. A. GAUSSIAN 92/DFT; Gaussian, Inc.: Pittsburgh, PA, 1993.
(26) Werner, H.-J.; Knowles, P. J. MOLPRO 94; University of Sussex: Falmer, Brighton, 1994.
(27) GAMESS (General Atomic and Molecular Electronic Structure System): Schmide, M. W.; Baldridge, K. K.; Boatz, J. A.; Jensen, J. H.; Koseki, S.; Gordon, M. S.; Nguyen, K. A.; Windus, T. L.; Elbert, S. T. *QCPE Bull.* **1990**, *10*, 52.
(28) Diau, E. W.; Lin, M. C.; Melius, C. F. *J. Chem. Phys.* **1994**, *101*, 3923.
(29) Berman, M. R.; Lin, M. C. *J. Phys. Chem.* **1983**, *87*, 3933.
(30) Hsu, D. S. Y.; Snaub, W. M.; Creamer, T.; Gutman, D.; Lin, M. C. *Ber. Bunsenges. Phys. Chem.* **1983**, *87*, 909.

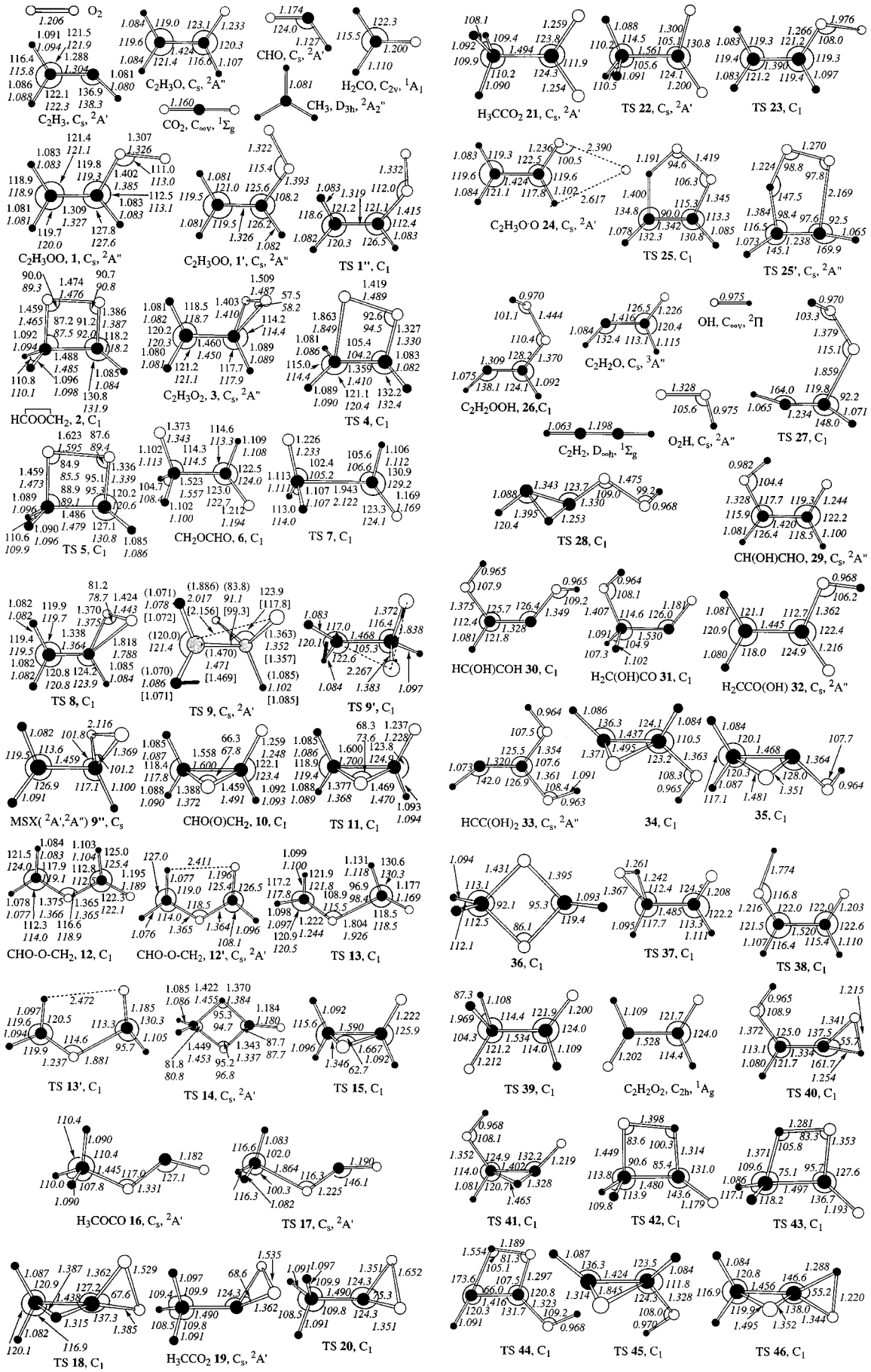

Figure 1. Optimized geometries (in Å and deg) of the reactants, products, various intermediates, and transition states for the $C_2H_3 + O_2$ reaction. Plain numbers for **1**−**15** show the parameters optimized at the UMP2/6-311G(d) level from ref 15b. The numbers in italics are optimized at the present B3LYP/6-311G(d,p) level. For **9**, the numbers in parentheses show UHF/6-311G(d) data (ref 15b), and the numbers in brackets are optimized at the CASSCF(7,5)/6-311G(d,p) level. Solid arrows for TS's **9** and **9′** show the normal mode corresponding to the imaginary frequency.

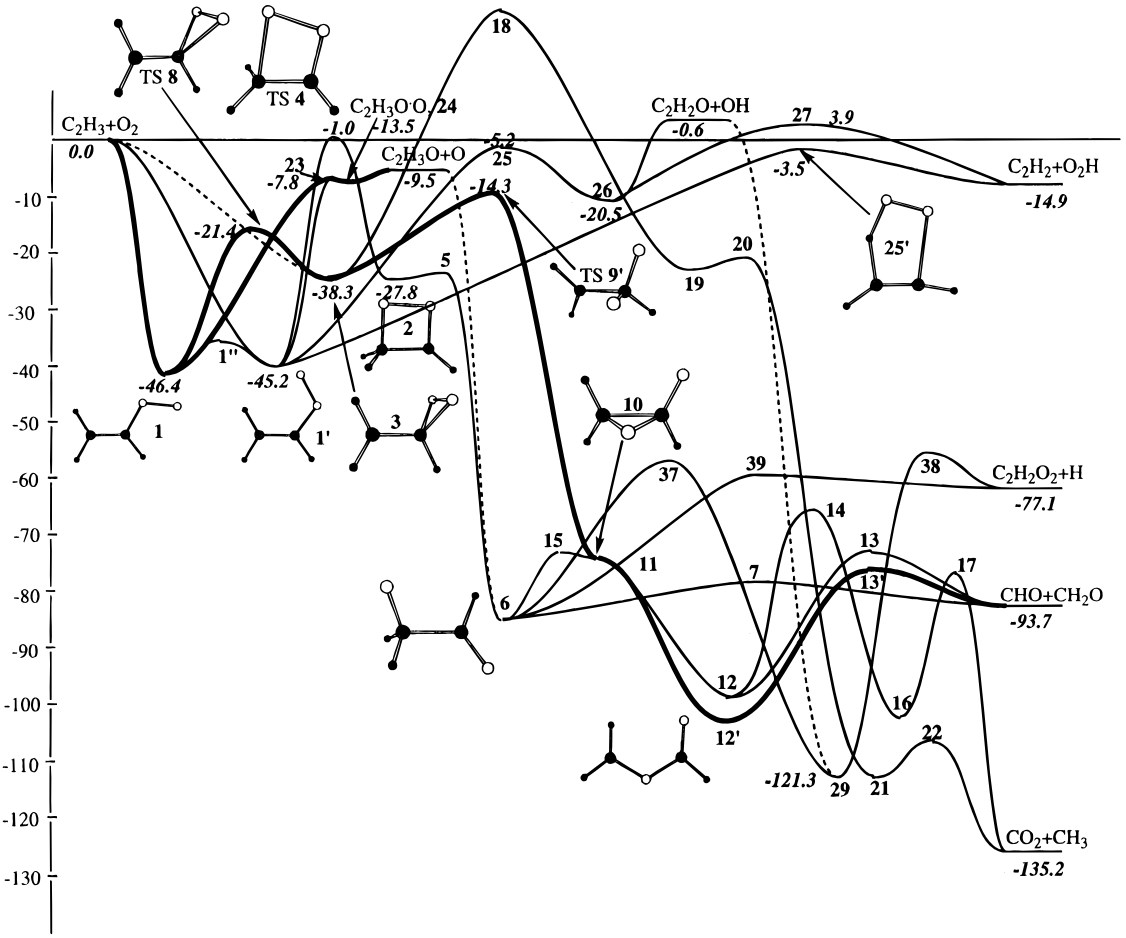

Figure 2. The profile of potential energy surface (in kcal/mol) for the most important mechanisms of the $C_2H_3 + O_2$ reaction. The energies of the curves are based on energies at the B3LYP/6-311G(d,p) + ZPE[B3LYP/6-311G(d,p)] level. Numbers in italics for some structures show energies at the higher level G2M(RCC,MP2) which include ZPE.

vinyl radical oxidation. We will at first examine the potential energy profile for this mechanism. We have found that this process proceeds from C_2H_3OO to **2** via a transition state **4**. The barrier is high; according to the PMP4/6-311G(d)//UMP2/6-311G(d)+ZPE results of Carpenter,[15] TS **4** lies about 14 kcal/mol above $C_2H_3 + O_2$. The present B3LYP/6-311G(d,p) + ZPE result gives the energy of 0.2 kcal/mol. The use of the G2M(RCC,MP2) method lowers the energy of **4** to −1.0 kcal/mol. Carpenter[15] considered only *trans* conformer **1** of C_2H_3-OO. Our IRC calculations showed that transition state **4** is connected to the intermediate **2** in the forward direction and to *cis*-C_2H_3OO, **1′**, in the reverse direction. If **1** is formed on the first reaction step, it has to rearrange into **1′** by rotation of OO around the single CO bond before going toward TS **4**. Transition state **1″** corresponds to the **1** → **1′** rotation with the barrier of 6.1 kcal/mol relative to **1** at the B3LYP/6-311G-(d,p)+ZPE level.

Intermediate **2**, dioxetanyl radical, which is formed after TS **4** is cleared, is less stable than **1** and lies 27.8 kcal/mol below the reactants at the G2M(RCC,MP2) level. A weak OO bond in the four-member ring of **2** can be easily broken, with the transfer of the oxygen to the second carbon and the formation of 2-oxoethoxy radical, intermediate **6**. **5** is the corresponding transition state. The **2** → **6** isomerization is highly exothermic, with the energy gain of about 70 kcal/mol. The barrier is low, only 1.2 kcal/mol at the B3LYP/6-311G(d,p) level, and TS **5** possesses an early character. Isomer **6** has no symmetry. Both *cis* and *trans* configurations of the 2-oxoethoxy radical with C_s symmetry have one imaginary frequency corresponding to the rotation around the CC bond. IRC calculations confirmed the connection of **2** with the asymmetric *trans*-**6** via TS **5**.

6 can give the reaction products CHO + CH_2O by scission of the CC bond. This process is nearly thermoneutral; PMP4 approximation with 6-311G(d),[15] 6-311G(d,p), and 6-311+G-(d,p) basis sets shows the exothermicity of 2.5−4.4 kcal/mol, but at the B3LYP/6-311G(d,p) level, an endothermicity of 2.8 kcal/mol is calculated. The barrier between **6** and CHO + CH_2O at transition state **7** is low again, 7.1 kcal/mol at the B3LYP level with respect to **6**. TS **7** has a loose geometry: the breaking CC bond length is 1.94 and 2.12 Å at the UMP2 and B3LYP levels, respectively. When compared with the UMP2 level, endothermicity of the **6** → CHO + CH_2O step in the B3LYP level causes elongation of the CC distance and gives a late character to the transition state.

The reaction mechanism just examined, $C_2H_3 + O_2$ → **1′** → **4** → **2** → **5** → **6** → **7** → CHO + CH_2O, has as the rate-determining step the formation of four-member-ring dioxetanyl radical **2**. Transition state **4** lies slightly below the reactants, and this channel would exhibit a small negative temperature dependence of the rate constant. The calculated reaction exothermicity, 93.7 kcal/mol at the G2M(RCC,MP2) level, significantly exceeds the experimental value of 87.5 kcal/mol. This error, unusually large for this high level of calculation, is a result of error accumulation. For the reactants, C_2H_3 and O_2, G2M(RCC,MP2) atomization energy is underestimated by 2.5 and 1.8 kcal/mol, respectively, as compared to experiment, while for the products, HCO and H_2CO, the calculated

Table 1. Relative Energies and ZPE (in kcal/mol) for Various Species through the $C_2H_3 + O_2$ Reaction, Calculated at Different Levels of Theory at the B3LYP/6-311G(d,p) Optimized Geometries

species	ZPE[a]	B3LYP/ 6-311G(d,p)	PMP4/ 6-311G(d,p)	PMP4/ 6-311+G(d,p)	RCCSD(T) 6-311G(d,p)	G2M(RCC,MP2)	exper[b]
$C_2H_3 + O_2$[c]	25.1(0)	0.0	0.0	0.0	0.0	0.0	0.0
$C_2H_3O + O$	26.6(0)	−5.1	−10.0	−11.3	−11.1	−9.5	−9.0
$CHO + CH_2O$	24.7(0)	−82.7	−86.8	−88.4	−85.8	−93.7	−87.5
$CO_2 + CH_3$	26.0(0)	−126.7	−132.0	−130.7	−128.1	−135.2	−131.1
H(O)CC(O)H + H	23.1(0)	−62.2	−68.9	−70.3	−68.5	−77.1	
$C_2H_2 + O_2H$	25.8(0)	−7.7	−4.5	−5.4	−7.7	−14.9	−13.4
C_2H_3OO, *trans*, **1**, C_s	29.8(0)	−41.2	−33.9	−34.4	−37.1	−46.4	
C_2H_3OO, *cis*, **1′**, C_s	29.9(0)	−40.1	−32.9	−33.2	−36.2	−45.2	
TS **1″**, C_1	29.5(1)	−35.1					
$HCOOCH_2$, **2**, C_1	30.2(0)	−15.2	−12.9	−14.0	−15.5	−27.8	
$C_2H_3(O_2)$, **3**, C_s	28.9(0)	−24.3	−25.3	−26.4	−26.0	−38.3	
TS **4**, C_1	28.6(1)	0.2	10.6	8.6	5.0	−1.0	
TS **5**, C_1	28.9(1)	−14.0	−5.8	−7.1			
CH_2OCHO, **6**, C_1	29.0(0)	−85.5	−82.4	−84.0			
TS **7**, C_1	26.9(1)	−78.4	−77.7	−79.8			
TS **8**, C_1	28.5(1)	−15.3	−11.0	−11.9	−10.6	−21.4	
TS **9**, C_s	28.1(1)	−28.0	−22.2	−24.6	−25.1	−34.0	
TS **9′**, C_1	28.0(1)	−9.5	−1.6	−3.3	−6.4	−14.3	
seam **9″**, $^2A'$	27.3(1)	−12.2	−5.9	−8.6	−7.9	−15.4	
$^2A''$	27.8(1)	−11.7	13.6	9.8	−1.8	−12.8	
$CHO(O)CH_2$, **10**, C_1	29.5(0)	−74.4	−71.8	−73.8			
TS **11**, C_1	8.8(1)	−74.8	−73.6	−75.6			
CHO−O−CH_2, **12**, C_1	29.1(0)	−98.7	−97.7	−99.1			
CHO−O−CH_2, **12′**, C_s	29.2(0)	−103.1	−101.7	−102.9			
TS **13**, C_1	26.8(1)	−72.8	−67.5	−69.5			
TS **13′**, C_1	27.6(1)	−75.9	−71.3	−73.5			
TS **14**, C_1	27.0(1)	−64.3	−65.1	−66.0			
TS **15**, C_1	29.2(1)	−73.9	−71.0	−73.2			
H_3COCO **16**, C_s	30.5(0)	−102.9					
TS **17**, C_1	27.8(1)	−75.8					
TS **18**, C_1	25.8(1)	28.2					
H_3CCO_2 **19**, C_s	29.5(0)	−23.6					
TS **20**, C_1	29.0(1)	−20.6					
H_3CCO_2 **21**, C_s	29.8(0)	−112.2					
TS **22**, C_s	28.8(1)	−107.8					
TS **23**, C_1	27.3(1)	−6.6	−6.5	−8.0	−5.0	−7.8	
C_2H_3O·O **24**, C_s	27.2(0)	−7.9	−10.8	−12.0	−10.5	−13.5	
TS **25**, C_1	25.9(1)	−0.6	5.4	4.2	4.0	−5.2	
TS **25′**, C_s	25.3(1)	−0.6	5.3	4.9	5.8	−3.5	
C_2H_2OOH, **26**, C_1	28.5(0)	−10.2	−7.2	−8.6	−9.4	−20.5	
$C_2H_2O(^3A'') + OH$	23.6(0)	4.2	4.3	0.9	1.7	−0.6	
TS **27**, C_1	26.7(1)	6.9	13.3	11.2	13.4	3.9	
TS **28**, C_1	25.8(1)	30.1					
$C_2H_2(OH)O$, **29**, C_s	31.1(0)	−112.7	−108.6	−110.6	−109.3	−121.3	
HC(OH)COH **30**, C_1	30.8(0)	−70.1					
$H_2C(OH)CO$ **31**, C_s	30.5(0)	−98.1					
$H_2CCO(OH)$ **32**, C_s	30.2(0)	−119.3	−119.4	−121.1			
$HCC(OH)_2$ **33**, C_s	25.8(0)	−72.4					
34, C_1	30.6(0)	−67.1					
35, C_1	30.7(0)	−67.4					
36, C_s	31.3(0)	−66.7					
TS **37**, C_1	26.6(1)	−56.1	−54.4	−57.0			
TS **38**, C_1	23.9(1)	−54.6	−55.0	−58.0			
TS **39**, C_1	23.8(1)	−59.3	−61.0	−62.8			
TS **40**, C_1	26.6(1)	−34.1					
TS **41**, C_1	28.0(1)	−64.4					
TS **42**, C_s	26.8(1)	−56.7					
TS **43**, C_s	26.8(1)	−79.6					
TS **44**, C_1	26.8(1)	−51.1					
TS **45**, C_1	29.8(1)	−62.2					
TS **46**, C_1	27.1(1)	−31.9					

[a] The energy values in the table include the ZPE correction. ZPE is calculated at the B3LYP/6-311G(d,p) level, with the number in parentheses representing the number of imaginary frequencies, NIMAG. [b] Experimental data from ref 32. [c] The total energies (in hartree) for the $C_2H_3 + O_2$ system are the following: B3LYP/6-311(d,p) −228.29181, PMP4/6-311G(d,p) −227.74462; PMP4/6-311+G(d,p) −227.75423; RCCSD(T)/6-311G(d,p) −227.75054; and G2M(RCC,MP2) −227.89624.

atomization energy is overestimated by 0.3 and 1.6 kcal/mol, respectively, causing the total error of 6.2 kcal/mol.

As seen in Figure 1, UMP2 and B3LYP methods give, in general, similar geometries for the intermediates and transition states **1**−**7**. However, sometimes the differences are significant; for example, the B3LYP optimized CC and OO bond lengths in **4** are 0.07 and 0.05 Å longer than the UMP2 optimized ones. The largest deviation is found for the CC distance in **7** where the B3LYP value is 0.18 Å longer than the UMP2 one. This is caused by the flatness of the potential energy surface. The change of the distance from 1.94 to 2.12 Å leads to the energy change of only 0.1 kcal/mol. Because the B3LYP relative

energies are closer to the G2M(RCC,MP2) energies than the UMP2 values and the UHF wavefunction for this species is susceptible to high-spin contamination, we consider B3LYP geometries as more reliable.

B. Three-Member-Ring Reaction Mechanisms. Carpenter[15] has suggested for the $C_2H_3 + O_2$ reaction another mechanism which involves an intermediate **3** with a CO_2 three-member ring. In **3**, carbon and hydrogen atoms form a symmetry plane and two oxygens are reflected by this plane. The CC π-bond breaks and the radical center is moved to the π-orbital of the terminal C. The OO bond becomes a single bond, with a length 0.16 Å longer than that in **1**. The dioxiranylmethyl radical **3** which lies 38.3 kcal/mol below the reactants at the G2M(RCC,MP2) level is 8.1 kcal/mol less stable than **1**. The transition state **8** separates **3** from **1** or **1′**; the barrier from **1** is 25.0 kcal/mol, much lower than the barrier for four-member cyclization at TS **4**. **8** is 21.4 kcal/mol lower than $C_2H_3 + O_2$ at the G2M(RCC,MP2) level. Due to the endothermicity of the **1** → **3** isomerization, TS **8** has a rather late character. The OO bond in **8**, for instance, is only 0.04 Å shorter than that in **3**, but is 0.12 Å longer than that in **1**. The COO angle changes by 34° from **1** to **8** and by 20° from **8** to **3**. In the reverse direction, TS **8** is connected to both *trans*- and *cis*-C_2H_3-OO because the potential energy surface bifurcates. Intermediate **3** has also been confirmed to be directly accessible from the reactants. If the $C_2H_3 + O_2 \rightarrow$ **3** reaction takes place within C_s symmetry, with C_2H_3 in-plane and O_2 out-of-plane, it is symmetry-forbidden, because $C_2H_3 + O_2$ at infinite separation has a $^2A'$ electronic state. However, if the symmetry breaks, O_2 can attach to C_2H_3 forming **3** without any barrier. This would happen if O_2 approaches C_2H_3 asymmetrically and out-of-plane and the trajectory goes through the geometries having higher energies than TS **8**, bypasses TS **8**, and ends in **3**. We could not find any TS connecting **3** with the reactants, their optimization leads to the $C_2H_3 + O_2$ dissociation.

Starting from **3**, two reaction scenarios are possible. Carpenter[15] has considered one: the migration of an oxygen atom onto a bridging position with formation of the oxiranyloxy radical **10**. The other possibility of hydrogen migration will be discussed near the end of this section. The intermediate **10** is much more stable than **1**, **2**, or **3**; at the B3LYP/6-311G(d,p) + ZPE level it lies 74.4 kcal/mol below the reactants. One of the oxygen atoms in **10** asymmetrically bridges the CC bond, and the radical center shifts onto the terminal oxygen. Carpenter could not find the transition state between **3** and **10**. He located a TS **9** only at the UHF level, and its PMP4 energy was lower than the energy of **3**. Based on this, Carpenter suggested that the dioxiranylmethyl radical **3** might not be a local minimum at the correlated level. Starting from the UHF geometry reported by Carpenter, we have found TS **9** at the B3LYP/6-311G(d,p) level. The energy of **9** actually is lower than the energy of **3** at the B3LYP level. Therefore, this transition state cannot be connected to **3**. We carried out IRC calculations from **9** in forward and reverse directions. TS **9** was found to have C_s symmetry, with C_2H_3 in-plane and two oxygens out-of-plane. As seen in Figure 1, the normal mode corresponding to the imaginary frequency of **9** belongs to the a″ irreducible representation and a motion along this mode destroys the symmetry. Profiles of IRC in two directions have to be identical and both reverse and forward calculations result in the intermediate **10**. Thus, **9** connects **10** with **10** and serves as a transition state for terminal-bridge exchange of two oxygen atoms. The barrier for this degenerate rearrangement is high, 46.4 kcal/mol at the B3LYP + ZPE level. Using the Neuman projection (with 0° defined as the 12 o'clock position), one can consider the process **10** (enantiomer) → **9** → **10** as the rotation of the COHO group: O^a 360° (terminal) → 300° → 240° (bridged), O^b 120° (bridged) → 60° → 0° (terminal), and H 210° → 180° → 150°.

Table 2. Molecular and Transition-State Parameters Used in the RRKM Calculations

species or transition state	i	I_i (10^{-40} g cm^2)	ν_j (cm^{-1})
C_2H_3	A	3.6	713, 820, 918, 1046,
	B	25.9	1391, 1651, 3038, 3136,
	C	29.4	3236
O_2	A	19.5	1638
	B	19.5	
	C	0.0	
C_2H_3OO, **1**	A	16.3	141, 350, 571, 684, 874,
	B	172.4	906, 980, 1134, 1188, 1289,
	C	188.7	1408, 1672, 3165, 3212, 3263
C_2H_3OO, **1′**	A	39.1	199, 337, 631, 689, 883,
	B	123.4	919, 969, 1071, 1176, 1320,
	C	162.5	1399, 1650, 3173, 3221, 3273
$C_2H_3O_2$, **3**	A	42.7	260, 395, 454, 608, 778,
	B	109.7	782, 956, 1140, 1149, 1243,
	C	126.3	1403, 2463, 3125, 3161, 3278
TS **4**	A	58.8	307, 577, 698, 782, 881,
	B	72.1	1008, 1024, 1165, 1226, 1397,
	C	123.2	1507, 3091, 3166, 3198
TS **8**	A	41.6	267, 480, 580, 839, 855,
	B	119.0	942, 969, 1193, 1280, 1383,
	C	133.3	1513, 3161, 3189, 3269
TS **9′**	A	57.4	293, 396, 466, 754, 882,
	B	95.7	953, 1140, 1215, 1235, 1371,
	C	127.5	1461, 3022, 3145, 3271
TS **23**	A	34.0	83, 190, 496, 584, 857,
	B	202.8	966, 1012, 1199, 1322, 1423,
	C	211.2	1490, 3039, 3146, 3257
TS **25**	A	47.7	459, 466, 639, 784, 851,
	B	94.6	893, 917, 945, 1129, 1214,
	C	141.5	1531, 1846, 3180, 3269
TS **25′**	A	46.0	286, 365, 587, 639, 680,
	B	136.1	731, 825, 862, 1055, 1343,
	C	182.1	1675, 1885, 3312, 3438

We have found TS **9′** which actually connects **3** with **10**. In **9′**, one of the oxygens is moved toward the CH_2 carbon, C^2; the OO distance is stretched from 1.49 Å in **3** to 1.84 Å in **9′** and the C^2O distance is shortened to 2.27 Å. In this sense, **9′** is an early TS because in **10**, the C^2O bond length is 1.39 Å. The process **3** → **9′** → **10** can be considered as the synchronous rotation of O^a 330° → 285° → 240°, O^b 30° → 15° → 0°, and H on C^2 180° → 165° → 150°. The barrier for the **3** → **10** isomerization via **9′** is calculated to be 24.0 kcal/mol, and the transition state lies 14.3 kcal/mol below the reactants at the G2M(RCC,MP2) level. Thus, **9′** is about 7 kcal/mol higher than **8**. Using molecular parameters shown in Table 2, we calculated entropies and Gibbs free energies for TS's **8** and **9′**. In the temperature range of 300−3500 K, the entropy of **9′** is slightly, by 0.4−0.7 cal·mol^{-1}·deg^{-1}, higher than the entropy of **8**. Meanwhile, the Gibbs free energy of TS **9′** is by 5−7 kcal/mol higher than that of TS **8**. Therefore, the **3** → **9′** → **10** isomerization, but not **1** → **8** → **3**, is the rate-determining step for the formation of CHO + CH_2O.

In addition to TS **9** within C_s symmetry that connects **10** and **10**, and TS **9′** in C_1 symmetry that connects **3** and **10**, there still may be a transition state in the vicinity of **9** that connects from **3** to **10**. A candidate is an asynchronous structure with O^a and O^b at 330° and 30° corresponding to **3** but the CO distances shortened as in **9**. TS **9** is in the $^2A'$ state with $(a'')^2(a')^1$ configuration and **3** in the $^2A''$ state has the $(a'')^1(a')^2$ configuration. Therefore, we at first located the minimum of the seam of crossing (MSX) between $^2A''$ and $^2A'$ electronic states within C_s symmetry, the structure **9″**. At the B3LYP/6-311G(d,p) level, **9″** lies 13.7 and 16.6 kcal/mol higher than **3**

and **9**, respectively. A B3LYP TS search without symmetry constraint starting from the neighborhood of **9″** converged to **9**, indicating that the hypothetical TS between **3** and **10** does not exist. A similar search using the CASSCF(7e,5o) method without symmetry constraints starting around **9″** converges to the structure, very similar to **9**, which is a TS for **10** → enantiomer **10** scrambling, but not for **3** → **10** isomerization. Therefore, we conclude that an asynchronous **3** → **10** transition state does not exist and the isomerization can take place only via the synchronous TS **9′**.

The reaction evolution starting from intermediate **10** can occur by two different paths. One is the migration of the bridging oxygen to C^2, giving the 2-oxoethoxy radical **6**. The transition state for this O-shift is structure **15** and the barrier is only 0.5 kcal/mol with respect to **10** at the B3LYP/6-311G(d,p) + ZPE level. The **10** → **6** isomerization is calculated to be exothermic by 11.1 kcal/mol at the B3LYP level, and TS **15** has an early character. The length of the breaking C^2O bond in **15** is by 0.21 Å longer than that in **10**, but by 0.77 Å shorter than that in **6**. Intermediate **6** can produce CHO + CH_2O via TS **7** with a low barrier, as was already discussed.

The other path, a breach of the CC bond with the formation of formyloxymethyl radical **12**, has been considered by Carpenter[15] and is more favorable than the first one. **11** is the transition state for the breach of the CC bond in **10**. At the B3LYP/6-311G(d,p) level, **11** is only 0.3 kcal/mol higher than **10**. With ZPE, TS **11** lies even 0.4 kcal/mol lower than **10**, indicating instability of the latter. The formyloxymethyl radical can exist in two conformations. Carpenter has calculated one of them, **12**, with the oxygen atom of C^1 in the *trans*-position relative to C^2. Structure **12** has no symmetry. We have found that another conformation, **12′**, with the terminal oxygen in the *cis*-position, is 4.4 kcal/mol more stable than **12** owing to the O···H hydrogen bond interaction with the OH distance of 2.41 Å. Both **12** and **12′** can be obtained from **10** via TS **11** because the potential energy surface is expected to have a bifurcation point after **11**. **12** and **12′** can rearrange to each other by rotation around the single OC bond, and the barrier would not be high. **12′** has C_s symmetry and $^2A''$ electronic state. In both conformations the unpaired electron is located on the CH_2 carbon. The **10** → **12** or **12′** isomerization is exothermic by 24.3−28.7 kcal/mol at the B3LYP+ZPE level.

The formyloxymethyl radical can dissociate by breaking the OC bond and giving the reaction products, CHO + CH_2O. *trans*-**13** and *cis*-**13′** transition states connect **12** and **12′**, respectively, with CHO + CH_2O. This reaction step is endothermic by 11−16 kcal/mol at different levels of theory. The transition states are late and loose, with the OC distance of 1.88−1.93 Å at the B3LYP level. The B3LYP OC bond length in **13** is 0.12 Å longer than the UMP2 optimized value, but the difference is attributable to the flatness of the potential energy surface. The energy of **13′** is by 3.1 kcal/mol lower than that of **13** at the B3LYP + ZPE level.

Another path of transformation of **12** is 1,3-hydrogen shift from C^1 to C^2 via transition state **14**. TS **14** lies somewhat higher than TS **13**, by 8.5, 2.4, and 3.5 kcal/mol at the B3LYP/6-311G(d,p), PMP4/6-311G(d,p), and PMP4/6-311+G(d,p) levels. IRC descent in the forward direction from **14** gives intermediate **16**, methoxyformyl radical H_3COCO. **16** is 4.2 kcal/mol more stable than **12** and 102.9 kcal/mol below the reactants, $C_2H_3 + O_2$. H_3COCO has C_s symmetry, with the symmetry plane containing four heavy atoms and one hydrogen, while two other hydrogens are reflected by the plane. The electronic state of **16** is $^2A'$ and the unpaired electron is located on a σ-orbital of C^1. H_3COCO **16** finally dissociates to CH_3 + CO_2, and the transition state is **17**. The latter has C_s symmetry, the breaking CO bond is elongated from 1.45 Å in **16** to 1.86 Å in **17**, and the OCO angle opens from 127.1° in **16** to 146.1° in **17** directing toward the linear CO_2 molecule. The barrier with respect to **16** is quite high, 27.1 kcal/mol at B3LYP+ZPE, but TS **17** lies 11.5 kcal/mol lower than TS **14** in this approximation. Meanwhile, the reverse reaction $CO_2 + CH_3$ → **17** → **16** has a high barrier of 50.9 kcal/mol.

The second reaction pathway from dioxiranylmethyl radical **3** leading to $CO_2 + CH_3$ also exists. Instead of oxygen migration to the bridging position, **3** → TS **9′** → **10** discussed above, this intermediate **3** can undergo a 1,2-hydrogen shift from C^1 to C^2. In this case, intermediate **19**, methyldioxiranyl radical H_3CCO_2, is formed via transition state **18**. While **18** is nonsymmetric, **19** has C_s symmetry and $^2A'$ electronic state. During the hydrogen shift, the radical center is moved in the opposite direction, from C^2 to C^1. **19** is only 0.7 kcal/mol less favorable than **3** at the B3LYP+ZPE level. The barrier for hydrogen shift is high, 52.5 kcal/mol, and TS **18** lies 28.2 kcal/mol above the reactants and 37.7 kcal/mol higher than TS **9′** at the B3LYP+ZPE level. Thus, this mechanism cannot compete with oxygen migration leading to **10**. The intermediate **19** can be transformed further by breaking the OO bond which results in the acetoxy radical **21**. This isomerization is highly exothermic; **21** lies 88.6 and 112.2 kcal/mol below **19** and $C_2H_3 + O_2$, respectively, at the B3LYP+ZPE level. **21** possesses C_s symmetry with carbon, oxygen, and one-hydrogen atoms in the plane of symmetry, and the electronic state is $^2A'$. The structure **20** is the transition state for the OO breach, between **19** and **21**. The barrier is low, 3.0 kcal/mol with respect to **19**, and **20** is an early transition state. Intermediate **19** is quasi-stable; once it is formed, it easily isomerizes to the acetoxy radical **21**. The rupture of the CC bond in the latter gives $CH_3 + CO_2$. This reaction step is exothermic by 14.5 kcal/mol (B3LYP+ZPE) and has an early transition state **22**. The latter has the same symmetry and electronic state as **21**. The barrier with respect to **21** is calculated to be 4.4 kcal/mol. The early character of **22** is seen in that the CC distance and OCO angle increase only by 0.07 Å and 18.9° as compared to those in **21**. The IRC calculation confirmed the connection of **22** with **21** and $CH_3 + CO_2$. For the reverse reaction, the barrier at TS **22** is 18.9 kcal/mol. Therefore, the reaction of CO_2 with CH_3 is more likely to produce **21** with the carbon atom of methyl forming a CC bond than **16** with formation of a new CO bond.

The reaction mechanisms involving the three-member-ring intermediate **3** can be summarized as follows:

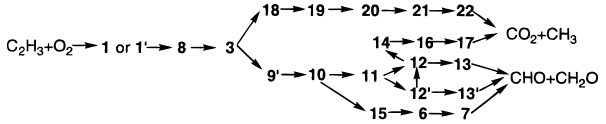

The channels leading to the CHO + CH_2O products are preferable because TS **9′** lies much lower than TS **18**, the barriers at TS **13** and **13′** are lower than that at TS **14**, and CHO + CH_2O can also be formed via the **10** → **15** → **6** → **7** subchannel with low barriers at TS's **15** and **7**.

C. Elimination of Oxygen Atom from the Vinylperoxy Radical. C_2H_3OO **1** or **1′** can dissociate with elimination of one oxygen atom, instead of undergoing complex rearrangement described in the previous two sections. The dissociation products, vinoxy radical and the O atom, lie 9.5 kcal/mol below $C_2H_3 + O_2$ at the G2M(RCC,MP2) level. This level is in good agreement with the experimental heat of the reaction, 9.0 kcal/mol.[32] The calculated endothermicity of the $C_2H_3OO \rightarrow C_2H_3O + O$ process is 36.9 kcal/mol at G2M(RCC,MP2). If the

dissociation takes place within C_s symmetry, it is symmetry-forbidden because **1** has $^2A''$ electronic state and the overall electronic state of $C_2H_3O + O$ is $^2A'$. Therefore, we looked for the transition state for O elimination without symmetry constraint. The search leads to structure **23**. Consistent to the reaction endothermicity, TS **23** has a late character; the geometry of the C_2H_3O fragment is close to that in the free radical and the OO distance is long, 1.98 Å. In the reverse view point, the oxygen atom attacks the planar vinoxy radical from an out-of-plane position, with the OOCC dihedral angle of 115.9°. At the B3LYP/6-311G(d,p) level, **23** lies 2.2 kcal/mol below the products, vinoxy + O, implying the existence of a $C_2H_3O\cdot O$ complex. Such a complex **24**, planar and in $^2A'$ electronic state, was located. As compared to **23**, the OO distance is elongated further, to 2.39 Å. At the B3LYP/6-311G(d,p)+ZPE level, the energy of the complex formation from C_2H_3O and O is 2.8 kcal/mol, and the barrier at TS **23**, with respect to $C_2H_3O\cdot O$, is 1.3 kcal/mol. The use of the more accurate G2M(RCC,MP2) method somewhat changes the energetics. At this level, TS **23** lies 7.8 kcal/mol below $C_2H_3 + O_2$ but 1.7 kcal/mol higher than $C_2H_3O + O$ products. The complexation energy for $C_2H_3O\cdot O$ **24** is 4.0 kcal/mol at G2M(RCC,MP2). Thus, for the $C_2H_3 + O_2 \rightarrow$ **1** or **1′** → TS **23** → $C_2H_3O\cdot O$ **24** → $C_2H_3O + O$ reaction channel, TS **23** is the rate-determining TS. At our best G2M(RCC,MP2) level, this transition state lies below the reactants but 6.5 kcal/mol higher than TS **9′** for the rate-determining step of CHO + CH_2O formation. On the other hand, TS **23** has a looser structure and therefore has a higher entropy than **9′**. Hence, at high temperatures, the channel leading to $C_2H_3O + O$ can compete with the mechanisms producing CHO + CH_2O, as will be seen from our RRKM calculations later. It is worth mentioning that the reverse $C_2H_3O + O$ reaction can produce not only C_2H_3OO but also the 2-oxoethoxy radical **6**, if the oxygen attacks C^2. The $C_2H_3O + O \rightarrow$ **6** reaction is highly exothermic and has no barrier. The direct abstraction, $C_2H_3 + O_2 \rightarrow C_2H_3O + O$, cannot take place.

D. The Pathways Involving Hydrogen Shift in C_2H_3OO. Another possibility of transformation of *cis*-C_2H_3OO, **1′** is the 1,4-hydrogen shift from C^2 to the terminal oxygen. We have found two transition states for the hydrogen shift. One, TS **25**, leads to intermediate **26**, 2-hydroperoxyvinyl-HCC(H)(OOH). This isomerization is endothermic; **26** lies 24.7 kcal/mol higher than **1′** but 20.5 kcal/mol below the reactants at the G2M(RCC,-MP2) level. The geometry of **26** is not planar; the OH bond is rotated out of plane with the HOOC dihedral angle of 88.4°. The unpaired electron in **26** shifts to C^2. TS **25** has a structure with a CCOOH five-member ring. This is a late transition state that could be anticipated from the reaction endothermicity. The moving H atom is located much closer to O (1.19 Å) than to C^2 (1.40 Å). The barrier for the hydrogen shift is 40.0 kcal/mol with respect to **1′** and TS **25** is 5.2 kcal/mol lower in energy than the reactants at the G2M(RCC,MP2) level.

Three pathways of reorganization of **26** are conceivable. The first one is the elimination of the OH group to form a triplet C_2H_2O. The cleavage of the OO bond occurs without barrier. At the G2M(RCC,MP2) level, C_2H_2O ($^3A''$) + OH lies 19.9 kcal/mol higher than **26** and 0.6 kcal/mol lower than $C_2H_3 + O_2$. The triplet C_2H_2O has C_s symmetry and two unpaired electrons are located on the σ-orbital of C^2 and π-orbital of O. The second mechanism is the rupture of the CO bond resulting in $C_2H_2 + O_2H$. The **26** → $C_2H_2 + O_2H$ step is endothermic by 5.6 kcal/mol at the G2M(RCC,MP2) level. Acetylene and O_2H lie by 14.9 kcal/mol below the reactants at this level of theory. This number is in close agreement with the experimental value of 13.4 kcal/mol.[32] **27** is the transition for the dissociation of **26** to $C_2H_2 + O_2H$. the CO bond in **27** is lengthened to 1.86 Å and both HCC angles approach 180°. The barrier at the G2M(RCC,MP2) level is 24.4 kcal/mol with respect to **26**. TS **27** is 3.9 kcal/mol higher than the reactants. The third channel is the 1,2-H shift in **26** from one carbon atom to another with the transition state **28**. The barrier has a typical height of 40.3 kcal/mol with respect to **26** at the B3LYP/6-311G-(d,p)+ZPE level, and TS **28** is 30.1 kcal/mol above the reactants. Therefore, this mechanism is not probable. One could expect that the hydrogen shift in **26** leads to the formation of the H_2-CCOOH radical. However, optimization of this structure leads to the dissociation into $H_2C{=}C{=}O$ and OH. Thus, TS **28** connects **26** with the H_2CCO + OH products.

The second transition state for the 1,4-hydrogen shift in C_2H_3-OO, **1′** is **25′**. Opposite to **25**, the five-member CCOOH ring in **25′** has a loose geometry; the CO distance is 2.17 Å. On the product side, TS **25′** is directly connected to $C_2H_2 + O_2H$. On the reactant side, **25′** seems to be connected to $C_2H_3 + O_2$, i.e., to be a transition state for direct hydrogen abstraction. However, this is not the case. IRC calculation confirmed **25′** to be connected with **1′**. TS **25′**, lying by 3.5 kcal/mol below $C_2H_3 + O_2$, corresponds to the hydrogen shift accompanied by the cleavage of the CO bond and the formation of the triple C≡C bond. The energy of **25′** is by 1.7 kcal/mol higher at the G2M-(RCC,MP2) level than the energy of **25**. However, **25′** has a looser geometry and therefore higher entropy than **25**. $C_2H_2 + O_2H$ would be produced rather by the **1′** → **25′** → $C_2H_2 + O_2H$ channel than by the **1′** → **25** → **26** → **27** → $C_2H_2 + O_2H$ channel, because **27** lies by 7.4 kcal/mol higher than **25′** at the G2M(RCC,MP2) level. Also, if intermediate **26** is formed, it would rather dissociate to C_2H_2O ($^3A''$) + OH than to $C_2H_2 + O_2H$.

We have not found any transition state for direct hydrogen abstraction from C_2H_3 by O_2. We tried to locate one, using the initial geometry similar to **25′**, but with oxygen in the *trans* position relative to the carbon of CH, in order to avoid formation of the CO bond. However, the energy of such a structure is much higher than the energy of the reactants and the optimization does not result in any saddle point.

E. Other Isomers of $C_2H_3O_2$. The reaction mechanism described above do not necessarily involve all of the potential isomers of the $C_2H_3O_2$ radical. In this section, we consider various arrangements of four heavy atoms of the radical and different distributions of three hydrogens between them in order to generate most of the possible isomers of these species. The only assumptions made for this consideration is that carbon and oxygen atoms should have the valences of 4 and 2, respectively. Some high-energy isomers might be missed this way, but they are not expected to be important for the reaction.

With respect to the arrangement of C and O atoms, all configurations of $C_2H_3O_2$ can be divided into the groups shown in Chart 1.

All of the structures **29**−**36**, which we did not consider in the previous sections, appear to be minima on the potential energy surface with no imaginary frequencies. Their implications to the reaction mechanism are discussed below.

The isomer **29**, HOCHCHO, can be obtained in the reaction of OH with triplet C_2H_2O, if OH attacks the radical center of C^2 and a new C−OH bond is formed. The reaction is barrierless and highly exothermic, 116.9 and 120.7 kcal/mol at the B3LYP/6-311G(d,p)+ZPE and G2M(RCC,MP2) levels, respectively. At our best level G2M(RCC,MP2), **29** lies 121.3 kcal/mol below $C_2H_3 + O_2$. HOCHCHO, **29** has C_s symmetry, $^2A''$ electronic state, with three electrons forming π-bonds between C^2, C^1, and O. **29** can rearrange to structure **6** by 1,2-H shift from oxygen

Chart 1

1. Chain isomers
   a. CCOO chain—structures **1**, **1′** and **26**.
      $H_2C{=}C{-}O{-}OH$ does not exist
   b. COCO chain—structures **12**, **12′**, and **16**
   c. COOC chain—no reasonable structures exist
   d. OCCO chain—structure **6**, and new isomers **29**, **30**, and **31**
2. Branch isomers—**21** as well as **32** and **33**

3. Three-member-ring isomers
   a. **3** and **19**

   b. **10**; **34** and **35**

4. Four-member-ring isomers
   a. Structure **2**

   b. New Isomer **36**

to C^2. **37** is the corresponding transition state. The rearrangement is endothermic by 27.2 kcal/mol, and the barrier is high, 29.4 and 67.6 kcal/mol relative to **6** and **29**, respectively, at the B3LYP+ZPE level. Isomer **29** can also eliminate the hydrogen atom of the OH group producing $C_2H_2O_2$ via the transition state **38**. The different conformations of **29** are not considered here, but the calculated one seems to be the most favorable one because of the stabilizing H···O interaction. Meanwhile, the global minimum for $C_2H_2O_2$ is H(O)C−C(O)H, diformyl acid, and has C_{2h} symmetry with two hydrogens located *trans* to each other. Therefore, hydrogen elimination via TS **38** is accompanied by the rotation about the single CC bond. As a result, **38** has no symmetry. The transition state has a late character. Its geometry is close to that of H(O)CC(O)H, except that the OCCO dihedral angle is different, and the OH distance is long, 1.77 Å. The endothermicity of the **29** → H(O)CC(O)H reaction is 50.5 and 36.2 kcal/mol at the B3LYP+ZPE and G2M(RCC,MP2) levels, respectively. At the B3LYP+ZPE level, the barriers for the hydrogen elimination from **29** and for the reverse reaction are 58.1 and 7.6 kcal/mol, respectively.

The H(O)CC(O)H + H products can also be formed by the hydrogen elimination from C^2 in the 2-oxoethoxy radical **6**. The barrier at transition state **39**, 26.6 kcal/mol with respect to **6** (B3LYP+ZPE), is significantly higher than the barrier for the dissociation of **6** to CHO + CH_2O at TS **7**, but 3.2 kcal/mol lower than the barrier for the **6** → **29** rearrangement via TS **37**. Thus, it is not likely that **29** can be obtained from the 2-oxoethoxy radical. If HOCHCHO, **29** is formed from C_2H_2O ($^3A''$) + OH, the two channels, **29** → TS **38** → H(O)CC(O)H + H and **29** → TS **37** → **6** → TS **7** → CHO + CH_2O, would compete, with the first more favorable than the second at high temperatures because their barriers are close and TS **38** is looser than TS **37**.

For the reaction of H(O)CC(O)H with H, the barrier at TS **39** for the formation of **6** is 4.7 kcal/mol lower than that at TS **38** for **29**. Thus, the main products of the H(O)CC(O)H + H reaction would be CHO + CH_2O, obtained by the following mechanism: H(O)CC(O)H + H → TS **39** → **6** → TS **7** → CHO + CH_2O.

The other isomers from group 1d are **30** and **31**. **30** has a rational formula HOCHCOH (vinyl-1,2-diol) and **31** is $HOCH_2$-CO (2-hydroxyacetyl radical). Neither structure has symmetry. The unpaired electron is located on C^1. **30** has a CC double bond and **31** has a C^1O double bond. Both **30** and **31** are less stable than **29**, by 42.1 and 14.1 kcal/mol at the B3LYP+ZPE level, respectively. Meanwhile, **31** is 12.6 kcal/mol more favorable than **6** and its energy is close to that of the formyloxymethyl radical **12** and **12′**. **30** can be obtained from **29** by the 1,2-hydrogen shift from C^1 to O via the transition state **40**. The barrier is calculated to be high, 36.0 and 78.6 kcal/mol relative to **30** and **29**, respectively, at the B3LYP+ZPE level. Although **30** seems to be kinetically stable, it would be extremely difficult to reach it from **29** or anywhere else. Intermediate **31** is connected to **29** and **6** through transition states **41** and **42**, respectively. **41** is a TS for the 1,2-H shift from one carbon atom to another. The barrier has a typical height of 33.7 kcal/mol at the B3LYP+ZPE level with respect to the less stable isomer **31**. **42** is a TS for the 1,3-hydrogen shift from the oxygen atom to C^1. The barrier for the 1,3-shift is 7.7 kcal/mol higher than that for the 1,2-shift reflecting higher exothermicity of the **31** → TS **41** → **29** reaction as compared to that of **31** → TS **42** → **6**. Intermediate **31** can also dissociate to hydroxymethyl radical CH_2OH and CO by the scission of the single CC bond, and the reverse barrier is expected to be similar to the barrier for the CH_3 + CO → CH_3CO reaction.

In addition to **21** discussed above, group 2 contains isomers **32** and **33**. **32** is $H_2CC(O)OH$ and lies 119.3 kcal/mol lower than $C_2H_3 + O_2$ (B3LYP+ZPE). We believe that **32** is the global minimum for the $C_2H_3O_2$ species. The $H_2CC(O)(OH)$ radical **32** is planar and its electronic state is $^2A''$. The unpaired electron belongs to the π-system and is distributed between C^1, C^2, and the terminal oxygen. TS **43** connects $H_2CC(O)OH$ with **21** and corresponds to the 1,3-hydrogen shift from C^2 to the oxygen atom. We did not consider all possible conformations of $H_2CC(O)OH$ assuming that **32** is the best one due to the H···O hydrogen bonding and rotation around the single CO bond is easy. TS **43** lies 32.6 and 39.7 kcal/mol higher than **21** and **32**, respectively. The pathway leading to the global minimum of $C_2H_3O_2$ is as follows: $CO_2 + CH_3$ → TS **22** → **21** → TS **43** → $H_2CC(O)(OH)$ **32**. The rate-determining step is the 1,3-H shift at TS **43** and the activation energy is 47.1 kcal/mol at the B3LYP+ZPE level. The reaction is endothermic by 7.4 kcal/mol.

Intermediate **33**, 2,2-dioxyvinyl radical $HCC(OH)_2$, is 46.9 kcal/mol less stable than **32**. Different conformations of HCC(OH) may exist, but **33** is probably the most stable one due to the H···O hydrogen bonds. **33** can be obtained from **32** by the 1,3-H shift from C^2 to the oxygen via transition state **44**. The barrier is calculated to be 21.3 and 68.2 kcal/mol relative to **33** and **32**, respectively, at the B3LYP+ZPE level.

Group 3b contains structures **10**, **34**, and **35** with one oxygen bridging the CC bond. **10** is the most stable of the three, and **34** and **35** lie by about 7 kcal/mol higher and are close in energy. In **34**, C^1 is bound with an H atom and hydroxyl, besides the bridging oxygen, and the radical center is located on C^2. This intermediate can be obtained from **29** by oxygen migration onto the CC bridge via TS **45**. The barrier, 50.5 kcal/mol with respect to **29**, is high but slightly lower than those at TS's **37** and **38** for rearrangement of **29** to **6** and dissociation to H(O)CC(O)H + H. However, **34** is not very stable kinetically; the reverse barrier for its transformation to **29** is only 4.9 kcal/mol.

In structure **35**, C^1 is connected to the OH group and has an impaired electron, while two other hydrogen atoms are connected to C^2. It can be reached from **10** by the 1,2-H shift from C^1 to the terminal oxygen. The barrier for the shift, located

at TS **46**, is 42.5 and 35.5 kcal/mol relative to **10** and **35**, respectively. Because **10** is not stable and rearranges to **6** or **12** virtually without barrier, **35** cannot be obtained through intermediate **10**. The other pathway leading to **35** would be oxygen migration to the bridging position in intermediate **32**. However, the **32** → **35** isomerization is endothermic by 51.9 kcal/mol and we do not consider this channel here.

Group 4b includes isomer **36** with a COCO four-member ring. The radical center is on C^1. The energy of **36** is close to those of **34** and **35**. **36** may also be connected with **10**, but due to the instability of the latter, we did not calculate this pathway.

F. Summary of Reaction Mechanisms. The profile of the potential energy surface for the most important channels of the $C_2H_3 + O_2$ reaction is shown in Figure 2. According to the energetics calculated at the G2M(RCC,MP2) and B3LYP/6-311G(d,p) levels, the most favorable pathway leading to the CHO + CH_2O products is the following: $C_2H_3 + O_2$ → **1** or **1′** → TS **8** → **3** → TS **9′** → **10** → TS **11** → **12** or **12′** → TS **13** or **13′** → CHO + CH_2O. The rate-determining step for this mechanism is oxygen migration to the CC bridging position vis TS **9′**, which lies 14.3 kcal/mol below the reactants at our best G2M(RCC,MP2) level. The alternative subchannel for the formation of these products is ...**10** → TS **15** → **6** → TS **7** → CHO + CH_2O. The $CO_2 + CH_3$ products can be formed from the formyloxymethyl radical **12**: ...**12** → TS **14** → **16** → TS **17** → $CO_2 + CH_3$. However, the energy of TS **14** is higher than that of TS **13′** by 6−11 kcal/mol at various levels of theory and the former has a much tighter geometry than the latter.

The main reaction products, CHO + CH_2O, can also be formed by the mechanism suggested earlier, involving a four-member-ring dioxetanyl radical **2**: $C_2H_3 + O_2$ → **1′** → TS **4** → **2** → TS **5** → **6** → TS **7** → CHO + CH_2O. The rate-controlling step is the formation of **2** via TS **4**, lying 1.0 kcal lower than the reactants and 13.3 kcal/mol higher than TS **9′** at the G2M-(RCC,MP2) level. Thus, this mechanism probably cannot compete with the channels involving the three-member-ring dioxiranylmethyl radical **3**.

The reaction can also proceed by the elimination of oxygen atom from the vinylperoxy radical **1** or **1′**: $C_2H_3 + O_2$ → **1** or **1′** → TS **23** → **24** → C_2H_3O + O. The transition state **23** is 6.5 kcal/mol higher in energy than TS **9′** (7.8 kcal/mol below the reactants), but its geometry is much looser than that of **9′**. Therefore, this channel can compete at high temperatures with the mechanisms going through TS **9′**. If the vinyloxy radical recombines with the oxygen atom, they can produce **6** without a barrier and the latter dissociates to CHO + CH_2O.

Hydrogen migration in C_2H_3OO, **1′** gives rise to other reaction channels: $C_2H_3 + O_2$ → **1′** → TS **25** → **26** → C_2H_2O ($^3A''$) + OH, where TS **25** and C_2H_2O + OH products lie 5.2 and 0.6 kcal/mol below the reactants at the G2M(RCC,MP2) level, and $C_2H_3 + O_2$ → **1′** → TS **25′** → $C_2H_2 + O_2H$ with TS **25′** lying by 3.5 kcal/mol below the reactants. These mechanisms are less favorable than those involving TS's **9′** and **23**. For the formation of C_2H_2O ($^3A''$) + OH, the hydrogen shift via TS **25** is rate determining, despite the fact that the products are higher in energy than the transition state. The **26** → C_2H_2O ($^3A''$) + OH dissociation is barrierless, and in the 300−3500 K temperature range the Gibbs free energy of TS **25** is always higher than that of C_2H_2O + OH. The intermediate **26** can also dissociate into $C_2H_2 + O_2H$ via TS **27**, which lies 3.9 kcal/mol above to the reactants; this channel would not be competitive at low temperatures. C_2H_2O ($^3A''$) + OH can recombine, producing very stable HOCHCHO intermediate **29**. HOCHCHO can either eliminate the hydrogen atom giving H(O)CC(O)H + H via TS **38** or rearrange into the 2-oxoethoxy radical **6** via TS **37**. The two transition states have close energies and these subchannels would be competitive.

G. RRKM Calculations of the Rate Constants for Key Product Channels. We have calculated the rate constants for formation of various products according to the following mechanisms:

$$C_2H_3 + O_2 \underset{-a}{\overset{a}{\rightleftharpoons}} C_2H_3OO^{\dagger}\ \mathbf{1} \xrightarrow{b\ (TS\ \mathbf{23})} C_2H_3O + O$$

$$\xrightarrow{c\ (TS\ \mathbf{25})} C_2H_2O + OH$$

$$\xrightarrow{d\ (TS\ \mathbf{25'})} C_2H_2 + O_2H$$

$$\xrightarrow{e\ (TS\ \mathbf{4})} CHO + CH_2O$$

$$\underset{-f}{\overset{f\ (TS\ \mathbf{8})}{\rightleftharpoons}} C_2H_3O_2^{\dagger}\ \mathbf{3} \xrightarrow{(TS\ \mathbf{9'})} CHO + CH_2O$$

$$\xrightarrow{h\ [M]} C_2H_3OO$$

where "†" represents the vibrational excitation of the peroxy and the dioxiranylmethyl radical intermediates. In the first approximation, we consider that the intermediate **3** derives solely from **1** through cyclization via TS **8** and is not formed directly from the $C_2H_3 + O_2$ association.

Steady-state assumption for both excited intermediates leads to the following expressions for the second-order rate constants of various product channels:

1. For channels b−e:

$$k_i(T) = \frac{\alpha_a}{h}\frac{Q_t^{\ddagger}\,Q_r^{\ddagger}}{Q_{C_2H_3}Q_{O_2}}e^{-E_a/KT}\int_0^{\infty}\frac{k_i(E)N_a(E^{\ddagger})e^{-E^{\ddagger}/KT}\,dE^{\ddagger}}{\omega + \sum k_j(E) - F(E)} \quad (I)$$

2. For the collisional stabilization of $C_2H_3OO^{\ddagger}$:

$$k_h(T) = \frac{\alpha_a}{h}\frac{Q_t^{\ddagger}\,Q_r^{\ddagger}}{Q_{C_2H_3}Q_{O_2}}e^{-E_a/KT}\int_0^{\infty}\frac{\omega N_a(E^{\ddagger})e^{-E^{\ddagger}/KT}\,dE^{\ddagger}}{\omega + \sum k_j(E) - F(E)} \quad (II)$$

3. For the formation of CHO + CH_2O via the ring intermediate **3**:

$$k_{f,g}(T) = \frac{\alpha_a}{h}\frac{Q_t^{\ddagger}\,Q_r^{\ddagger}}{Q_{C_2H_3}Q_{O_2}}e^{-E_a/KT}\int_0^{\infty}\frac{G(E)N_a(E^{\ddagger})e^{-E^{\ddagger}/KT}\,dE^{\ddagger}}{\omega + \sum k_j(E) - F} \quad (III)$$

where

$$k_i(E) = \alpha_i C_i N_i(E_i^{\ddagger})/\rho(E) \quad (IV)$$

$$F(E) = k_f(E)k_{-f}(E)/[k_{-f}(E) + k_g(E)] \quad (V)$$

$$G(E) = k_g(E)k_{-f}(E)/[k_{-f}(E) + k_g(E)] \quad (VI)$$

$$\sum k_j(E) = k_{-a}(E) + k_b(E) + k_c(E) + k_d(E) + k_e(E) + k_f(E) \quad (VII)$$

and

$$\omega = k_h[M] \quad (VIII)$$

In the above equations, α_i is the statistical factor for the ith reaction path, and E_a is the energy barrier for the formation of the vinyl peroxy radical via step a, which is effectively zero.

Table 3. Maximum $\Delta G^{\ddagger}$, the Corresponding $CO^{\ddagger}$ Distance, and the Rate Constant for Unimolecular Decomposition of C_2H_3OO, **1** ($C_2H_3OO \rightarrow C_2H_3 + O_2$) Calculated on the Basis of Canonical Variational Transition-State Theory

T, K	$CO^{\ddagger}$, Å	$\Delta G^{\ddagger}$, kcal/mol[a]	k_{-a}, s^{-1}
300	2.63	36.47	1.68×10^{-14}
500	2.51	33.80	1.75×10^{-2}
700	2.23	31.51	2.11×10^{3}
900	2.21	29.67	1.16×10^{6}
1000	2.21	28.80	1.05×10^{7}
1200	2.19	27.15	2.83×10^{8}
1400	2.18	25.61	2.92×10^{9}
1600	2.16	24.18	1.66×10^{10}
1800	2.15	22.87	6.26×10^{10}
2000	2.13	21.64	1.79×10^{11}
2200	2.12	20.52	4.19×10^{11}
2500	2.09	19.00	1.14×10^{12}
3000	2.06	16.87	3.68×10^{12}
3500	2.03	15.28	8.09×10^{12}

[a] At the B3LYP/6-311G(d,p) level, relative to C_2H_3OO, **1**.

$Q_{C_2H_3}$ and Q_{O_2} are the total partition functions of C_2H_3 and O_2, respectively, and $Q_t^{\ddagger}$ and $Q_r^{\ddagger}$ are the transitional and rotational partition functions of the association TS (a). $N_a(E^{\ddagger})$ is the sum of states of TS (a) with excess energy $E^{\ddagger}$ above the association barrier E_a, $k_i(E)$ is the specific rate constant[30] for the ith channel, and C_i is the ratio of the overall rotational partition function of the TS and the vinyl peroxy radical, which may be either *cis*- or *trans*-C_2H_3OO. Because of the small torsion barrier ($V_0 =$ 5 kcal/mol) and the large density of state, $\rho(E)$, due to the high internal energy carried by the excited C_2H_3OO radical ($\geq$46 kcal/mol), both the harmonic oscillator and the free internal rotor approximation for the C−OO torsional mode gave essentially the same result for the Gibbs free energy. The effective collision frequency ω, given by eq VIII, was calculated by Troe's weak-collision approximation.[31]

Our existing multichannel RRKM program prevoiusly employed for the $CH_3 + O_2$ reaction rate constant calculation[30] was modified for the present system. The evaluation of various rate constants given by eqs I−III is straightforward for all the steps, except the association process a which does not have a well-defined TS on account of the absence of reaction barrier. To circumvent the difficulty, we applied the much-practiced canonical variational method[33] based on the maximum free energy of activation, $\Delta G^{\ddagger}$. In order to find the maximum $\Delta G^{\ddagger}$ for each temperature, we first scanned the potential energy surface for the approach of O_2 to C_2H_3. We assumed that the oxygen molecule approaches the vinyl radical in-plane and in the *trans*-position. The CO distance was fixed at the values from 1.6 to 3.0 Å with the interval of 0.1 Å, and other geometric parameters were optimized for each value of CO. Thus, we calculated 15 optimized geometries for CO distances from 1.6 to 3.0 Å. For each structure, we calculated $3N - 7$ vibrational frequencies, projected out of the gradient direction. The computed B3LYP/6-311G(d,p) energies, moments of inertia, and vibrational frequencies (shown in supporting information for the most important 1.6−2.7 Å interval) were used for the calculations of ΔG. The B3LYP energies seem to be reliable enough because they change steadily and approach the energy of the separated fragments. Also, the B3LYP energy of the **1** $\rightarrow C_2H_3 + O_2$ reaction is close to the RCCSD(T) energy.

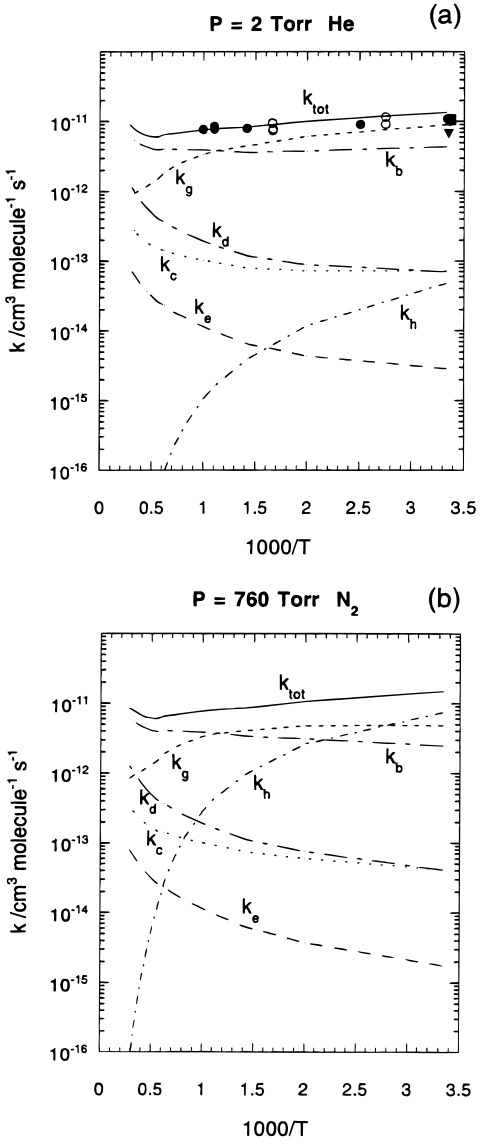

Figure 3. Arrhenius plots of the total and individual rate constants for the $C_2H_3 + O_2$ reaction and its various channels: k_{tot}, total rate constant, $C_2H_3 + O_2 \rightarrow$ products; k_b, $C_2H_3 + O_2 \rightarrow$ **1** or **1′** $\rightarrow$ TS **23** $\rightarrow C_2H_3O + O$; k_c, $C_2H_3 + O_2 \rightarrow$ **1′** $\rightarrow$ TS **25** $\rightarrow$ ... $\rightarrow C_2H_2O(^3A'') +$ OH; k_d, $C_2H_3 + O_2 \rightarrow$ **1′** $\rightarrow$ TS **25′** $\rightarrow C_2H_2 + O_2H$; k_e, $C_2H_3 + O_2 \rightarrow$ **1′** $\rightarrow$ TS **4** $\rightarrow$ CHO + CH_2O; k_g, $C_2H_3 + O_2 \rightarrow$ **1** or **1′** $\rightarrow$ TS **8** $\rightarrow$ **3** $\rightarrow$ TS **9′** $\rightarrow$ CHO + CH_2O; and k_h, $C_2H_3 + O_2$ (M) $\rightarrow$ **1** or **1′**. (a) At 2 Torr pressure of He: closed circles show experimental data at 1−6 Torr from ref 12. Open circles are experimental data at 0.3−3.5 Torr from ref 9. Squares designate experimental data at 0.4−4 Torr from ref 8. Triangles show experimental data at 400 Torr of He from ref 11. (b) At 760 Torr pressure of N_2. Key rate constant expressions are given in the text.

Because the structures with CO > 1.6 Å have one a″ vibrational frequency below 100 cm^{-1}, in the free Gibbs energy calculations, we substituted this frequency by free rotation around the CO axis. The reduced moment of inertia for the free rotation was computed from the geometry of each structure. The structures with CO longer than 2.1 Å have another low vibrational frequency. Therefore, we used the two-dimensional rotor for the ΔG calculations. We looked for the maximum $\Delta G^{\ddagger}$ for various temperatures in the range from 300 to 3500 K. The accurate position of the maximum for each temperature, calculated on the basis of the parabolic fit of the three largest ΔG values, is shown in Table 3. Using the maximum $\Delta G^{\ddagger}$, we calculated the VTST rate constant for the C_2H_3OO **1** $\rightarrow C_2H_3 + O_2$ decomposition, also shown in Table 3. This rate constant

(31) Troe, J. *J. Phys. Chem.* **1979**, *83*, 114.
(32) (a) Chase, M. W., Jr.; Davles, C. A.; Downey, J. R., Jr.; Frurip, D. J.; McDonald, R. A.; Syverud, A. N. JANAF Thermochemical Tables. *J. Phys. Chem. Ref. Data* **1985**, *14*, Suppl. 1. (b) *CRC Handbook of Chemistry and Physics*, 74th ed.; Lide, D. R., Ed.; CRC Press: Boca Raton, 1993.
(33) (a) Garret, B. C.; Truhlar, D. G. *J. Chem. Phys.* **1979**, *70*, 1593. (b) Isaacson, A. D.; Truhlar, D. G. *J. Chem. Phys.* **1982**, *76*, 1380.

Table 4. Calculated Total and Individual Rate Constants for the $C_2H_3 + O_2$ Reaction (10^{-12} cm^3 molecules^{-1} s^{-1}) at the Pressure (760 Torr) of N_2

T, K	k_b	k_c	k_d	k_e	k_g	k_h	k_{tot}
300	2.447	4.152×10^{-2}	4.109×10^{-2}	1.760×10^{-3}	4.845	7.390	14.80
500	3.092	5.999×10^{-2}	7.437×10^{-2}	3.735×10^{-3}	4.786	2.616	10.60
700	3.350	7.402×10^{-2}	1.114×10^{-1}	6.153×10^{-3}	4.054	9.775×10^{-1}	8.57
900	3.738	9.275×10^{-2}	1.633×10^{-1}	9.551×10^{-3}	3.595	4.270×10^{-1}	8.03
1000	3.836	1.005×10^{-1}	1.897×10^{-1}	1.320×10^{-2}	3.298	2.817×10^{-1}	7.72
1200	3.937	1.143×10^{-1}	2.441×10^{-1}	1.499×10^{-2}	2.725	1.241×10^{-1}	7.16
1400	3.997	1.277×10^{-1}	3.025×10^{-1}	1.889×10^{-2}	2.250	5.600×10^{-2}	6.75
1600	4.069	1.417×10^{-1}	3.664×10^{-1}	2.311×10^{-2}	1.885	2.603×10^{-2}	6.51
1800	3.903	1.476×10^{-1}	4.125×10^{-1}	2.616×10^{-2}	1.483	1.100×10^{-2}	5.98
2000	4.073	1.648×10^{-1}	4.893×10^{-1}	3.109×10^{-2}	1.314	5.492×10^{-3}	6.08
2200	4.275	1.836×10^{-1}	5.739×10^{-1}	3.648×10^{-2}	1.187	2.816×10^{-3}	6.26
2500	4.639	2.150×10^{-1}	7.163×10^{-1}	4.547×10^{-2}	1.057	1.082×10^{-3}	6.67
3000	5.392	2.763×10^{-1}	9.964×10^{-1}	6.296×10^{-2}	9.379×10^{-1}	2.450×10^{-4}	7.67
3500	5.954	3.289×10^{-1}	1.255	7.883×10^{-2}	8.399×10^{-1}	5.781×10^{-5}	8.46

is fitted to give the following expression:

$$k_{-a} = 4.40 \times 10^{15} \exp(-40062/RT)\ s^{-1}$$

In the RRKM calculations, we used for the transition state of step a the molecular parameters of the structure with a maximum $\Delta G^{\ddagger}$ for each temperature. As the maxima are located between the calculated structures, the corresponding moments of inertia and vibrational frequencies were linearly interpolated.

First, we compared the predicted values with the experimental data[8−12] and performed the RRKM calculations for the pressure of 2 Torr of He. The total and individual rate constants are shown in Figure 3a. The calculated k_{tot} is in quantitative agreement with experiment. At low pressure and temperatures below 900 K, the reaction is dominated by the formation of CHO + CH_2O through step g. At higher temperatures, the C_2H_3O + O channel takes over. Rate constant k_d, corresponding to the formation of $C_2H_2 + O_2H$, is the third by value, and at the temperatures of about 3000 K, it even becomes higher than k_g.

RRKM calculations have also been performed for atmospheric pressure with N_2 as the bath gas. The results are shown in Figure 3b and Table 4. At room temperature, the reaction is dominated by the stabilization of the vinylperoxy radical C_2H_3-OO. At 500 K, the CHO + CH_2O channel becomes the major one. At 900 K, the formation of C_2H_3 + O becomes dominant. The $C_2H_2 + O_2H$ product channel also has a high rate constant, and at temperatures higher than 3000 K, it is the second most significant channel. The total and most important individual rate constants are fitted by least squares to the following three-parameter expressions in cm^3 molecule^{-1} s^{-1} for 300−3500 K and 760 Torr of N_2:

$$k_{tot} = (9.15 \times 10^{-13}) T^{0.23} \exp(454.0/T)$$

$$k_g + k_e(\mathrm{CHO} + \mathrm{CH_2O}) = (7.60 \times 10^{-8}) T^{-1.39} \exp(-510.6/T)$$

$$k_b(\mathrm{C_2H_3O} + \mathrm{O}) = (5.03 \times 10^{-13}) T^{-0.29} \exp(-5.4/T)$$

$$k_d(\mathrm{C_2H_2} + \mathrm{O_2H}) = (2.22 \times 10^{-18}) T^{1.61} \exp(193.0/T)$$

$$k_h(\mathrm{C_2H_3OO}) = (5.06 \times 10^{12}) T^{-8.00} \exp(-2860.5/T)$$

Comparison of Figures 3a and 3b shows that the pressure dependence of the total rate constant is small.

Using detailed balancing on the basis of the calculated k_d and equilibrium rate constant for the $C_2H_3 + O_2 \rightarrow C_2H_2 + O_2H$ reaction, we also calculated the rate constant k_{-d} for the reverse $C_2H_2 + O_2H \rightarrow C_2H_3 + O_2$ reaction. k_{-d} is fitted in the temperature range of 300−3500 K by the following three-parameter expression:

$$k_{-d} = (5.18 \times 10^{-18}) T^{1.61} \exp(-7130.9/T)\ \mathrm{cm^3\ molecule^{-1}\ s^{-1}}$$

The two-parameter expression for the 300−1000 K temperature range is as follows:

$$k_{-d} = (7.45 \times 10^{-13}) \exp(-7970.6/T)\ \mathrm{cm^3\ molecule^{-1}\ s^{-1}}$$

This means that the apparent activation energy for the $C_2H_2 + O_2H \rightarrow C_2H_3 + O_2$ reaction, 15.8 kcal/mol, is close to the reaction endothermicity, 14.9 kcal/mol.

As discussed in section B, the dioxiranylmethyl radical **3** can be formed directly from $C_2H_3 + O_2$ through an asymmetric association pathway without barrier. Therefore, we searched for a variational transition state on the Gibbs free energy surface of the $C_2H_3 + O_2 \rightarrow$ **3** association using a similar approach as for the $C_2H_3 + O_2 \rightarrow$ **1** association. The distance between the reactive C atom of C_2H_3 and the center of the OO bond was fixed at different values and other geometric parameters were optimized without symmetry constraints. In all cases, such optimization converged to planar structures, i.e., to the variational TS's found earlier for the $C_2H_3 + O_2 \rightarrow$ **1** association. On this basis, we concluded that both $C_2H_3 + O_2 \rightarrow$ **1** and $C_2H_3 + O_2 \rightarrow$ **3** channels share the same variational TS. After the transition state, the ΔG surface can bifurcate leading to either peroxy **1** or dioxiranylmethyl radical **3**.

In order to test the effect of bifurcation in the initial association reaction, we assumed the bifurcation probability to be 50% for both $C_2H_3 + O_2 \rightarrow$ **1** and $C_2H_3 + O_2 \rightarrow$ **3** channels using the same TS parameters. The result of the RRKM calculation using similar rate constant expressions I−III by including the term for the direct formation of **3** gives virtually the same total reaction rate constant as without considering the direct formation of **3**. This is not surprising because the reaction is controlled by the association variational TS which does not change. Only minor changes have been found for the rates of individual channels. For instance, at 300 K and the pressure of 2 Torr of He the rate constant of the formation of CHO + CH_2O via TS **9′** (k_f) slightly decreases, from 8.94×10^{-12} to 8.65×10^{-12}, and the rate constant of the C_2H_3O + O channel (k_b) increases from 4.36×10^{-12} to 4.96×10^{-12}. Since the bifurcation factor is not well defined and the changes in the rate constants are small, we believe that our consideration of the approximation neglecting the direct formation of **3** from the reactants is valid as described.

IV. Concluding Remarks

The reaction mechanism involving the three-member-ring dioxiranylmethyl radical **3** is confirmed to be the most favorable for the vinyl radical oxidation. The critical transition state for this channel, **9′**, corresponds to the shift of an oxygen atom to the CC-bridging position and lies 14.3 kcal/mol below reactants at our best theory level, G2M(RCC,MP2). This mechanism produces CHO + CH_2O. The C_2H_3O + O products can be achieved through a competitive mechanism involving the decomposition of the vinylperoxy radical by the elimination of the oxygen atom. The critical TS **23** is 7.8 kcal/mol lower in energy than $C_2H_3 + O_2$. The $C_2H_2 + O_2H$ products can be formed by the 1,4-H shift in vinylperoxy radical **1′** accompanied by the cleavage of the CO bond and the formation of the triple C≡C bond. The respective TS **25′** lies by 3.5 kcal/mol below the reactants.

The low pressure constant calculated on the basis of RRKM theory is in quantitative agreement with experiment. At atmospheric pressure and room temperature, the reaction has been shown to be dominated by the stabilization of C_2H_3OO. In the 500−900 K temperature range, the CHO + CH_2O channel has the highest rate constant, and at $T \geq 900$ K, C_2H_3O + O are the major products. At very high temperatures, the channel producing $C_2H_2 + O_2H$ is the second most significant one.

Acknowledgment. The authors are thankful to the Cherry L. Emerson Center for Scientific Computation for the use of various programs and computing facilities. Helpful discussion with Dr. C. F. Melius is much appreciated. A part of the calculation has been performed on the supercomputer Cray C90 in the Pittsburgh Supercomputing Center with the Grant No. CHE940026P. A.M.M. and K.M. acknowledge the support received from the Air Force Office of Scientific Research through Grant F49620-95-1-0182. A.M.M. and M.C.L. acknowledge the support received from the Department of Energy, Office of Basic Energy Sciences, Division of Chemical Sciences through Contract DE-FGO5-91ER14191.

Supporting Information Available: Table of energies and molecular parameters for the $C_2H_3-O_2$ structures optimized at various CO distances (2 pages). See any current masthead page for ordering and Internet access instructions.

JA961476E